# Gap effects on whispering-gallery mode microresonances

Zhixiong Guo*[a], Haiyong Quan[a], Stanley Pau[b]
[a]Dept. of Mech. & Aerosp. Eng., Rutgers University, Piscataway, NJ, USA 08854
[b]Bell Labs, Lucent Technologies, Murray Hill, NJ, USA 07974

## ABSTRACT

Photon tunneling between an optical resonator and a light-delivery coupler is strongly dependent on the gap dimension which can vary from zero to size of an optical wavelength involved. In this systematic report, we investigate the gap effects of whispering-gallery modes in two modeling systems: a waveguide-coupling resonator of 2μm and 10μm in diameter, respectively. Maxwell's equations which govern the EM wave propagation and photon tunneling in the microsystems are solved using the finite element method. The simulation accuracy and sensitivity is examined. It is found that when the maximum element size in the computationally sensitive regions is below 1/8 of the wavelength involved, the calculations are accurate. An optimal gap exists for maximum energy coupling and is a strong function of the wavelength of the resonant mode. The *Q* factor increases exponentially with increasing gap and saturates as the gap approaches the optical wavelength. An optimum gap can be defined at the half maximum energy coupling where both the *Q* factor and coupling efficiency are high. We also calculate the effects of gap width on the resonance shift. We find that the resonance wavelength is increased (decreased) with decreasing gap width for the 10μm (2μm) diameter resonator with narrow gap widths.

**Keywords**: whispering-gallery modes, optical microresonances, gap effects, *Q* factor, coupling efficiency, optimum gap

## 1. INTRODUCTION

Optical whispering-gallery modes (WGMs) describe resonant electromagnetic modes of photons that circulate in well-defined trajectories inside a dielectric medium of circular geometry. WGMs occur when EM waves confined by the total internal reflection at the curved boundary of a cavity can close on themselves. Nussenzveig[1] found that if a spherical particle (as a resonator) is much larger than the wavelength of light involved, WGMs can be represented as geometric orbits. The resonance situation is then akin to a violin string, which supports vibrational modes only at those frequencies that provide for an integral number of half wavelengths along its length[2]. Hence, WGMs are morphology-dependent resonances[3]. The resonant wavelengths and frequencies are estimated approximately by:

$$2\pi r \approx \frac{m\lambda_m}{n} = \frac{mc_0}{f_m n} \tag{1}$$

where $r$ and $n$ are the radius and refractive index of the resonator, respectively; $m$ is an integer and represents the resonance mode; $\lambda_m$ and $f_m$ are the resonant wavelength and frequency at mode $m$, respectively. If a dielectric medium would have a dimension of the order of the wavelength, $r \sim \lambda_m$, and have negligible optical losses, a microcavity made of this medium could have a very small mode volume and high finesse.

An ideal cavity would confine light indefinitely (i.e., without loss) and would have resonant frequencies at precise values. In reality optical losses exist due to material absorption or scattering as a result of surface roughness or material inhomogeneity[4]. Ultimately the photon lifetime is limited by diffraction[2], which causes photon trajectories to be less certain, allowing the energy eventually to "leak" out. The resonant quality is described by the cavity *Q* factor that is defined as $2\pi$ times the ratio of the stored energy in the microcavity to its energy lost per optical period. Thus, the *Q* factor is proportional to the photon confinement time. In general, a resonant band has a Lorentzian lineshape; and the *Q* factor can be calculated by[3] $Q = \omega_0 / \Delta\omega$, where $\omega_0$ is the resonance central frequency and $\Delta\omega$ is the full-width at half

* guo@jove.rutgers.edu; phone 1 732 445-2024; fax 1 732 445-3124

Nanofabrication: Technologies, Devices, and Application II
edited by Warren Y.-C. Lai, Leonidas E. Ocola, Stanley Pau
Proc. of SPIE Vol. 6002, 600204, (2005) · 0277-786X/05/$15 · doi: 10.1117/12.628867

maximum (FWHM) of its Lorentzian lineshape. $Q > 10^9$ has been observed at red and near-infrared wavelengths in fused-silica microparticles[5, 6].

Another important parameter describing optical microcavities is finesse, which is defined as a ratio of the free-spectral range (FSR) to FWHM. The term FSR represents the interval between two adjacent resonant frequencies. With a cavity radius at 15 μm, the FSR can be as wide as 2 THz (over 10 nm)[7]. From Eq. (1), the FSR is inversely proportional to the cavity size. Microscale cavities ensure that resonant frequencies are more sparsely distributed throughout the cavity size-dependent resonant optical spectrum than they are in corresponding "mesoscale" and "macroscale" cavities. However, it should be aware of that the effects of diffraction grow as the cavity shrinks; and when the periphery of the cavity approaches the wavelength of light passing through the interior, resonances are lost altogether.

Different from Mie resonances in microdroplets of aerosols which are observable by means of elastic and inelastic scattering of free-space beams, high-*Q* WGMs are not accessible by free-space beams[8]; and therefore, require employment of near-field couplers. Numerous coupling devices, such as high-index prisms with frustrated total internal reflection[8], side-polished fiber couplers[9], tapered optical fibers tapers[10], and waveguides[11-14], have been developed by several research groups. The principle of all these devices is based on providing efficient energy transfer to the resonant circular TIR guided wave in the resonator through the evanescent field of a guided wave or a TIR spot in the coupler. It is evident *a priori* that efficient coupling can be expected on fulfillment of two main conditions: phase synchronism and significant overlap of the two evanescent fields in the gap between the microcavity and the coupler. Thus, the gap is a critical parameter that affects the coupling efficiency.

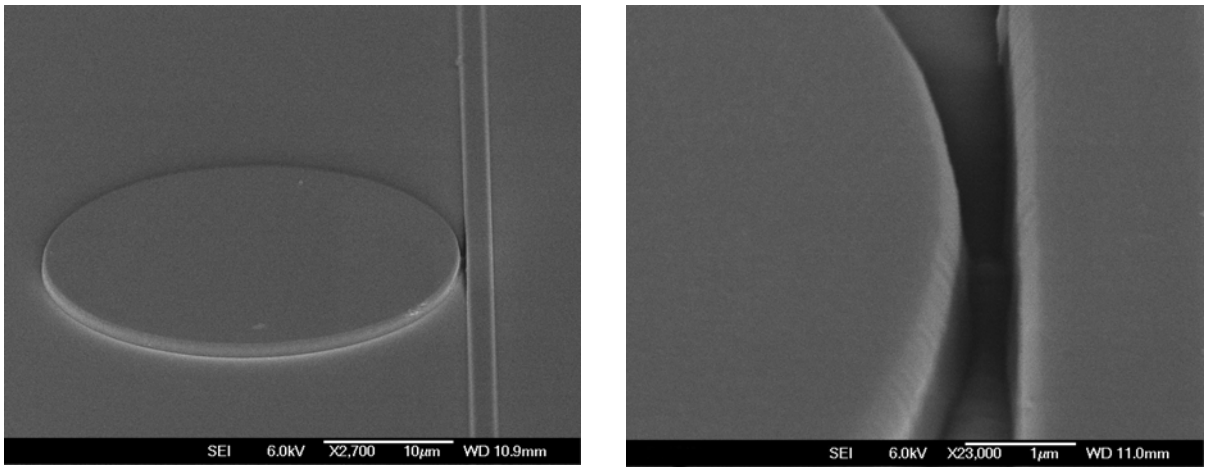


Figure 1. SEM images of a nanofabricated WGM microdevice consisted of a microdisk and a coupled waveguide.

It is tough to control the gap for lab-built WGM microresonant systems in which most are microsphere-optical fiber coupling systems. Recent advances in the technology of nanofabrication offer the possibility of manufacturing new optical devices with unprecedented control. It is now feasible to consider WGM microcavities, light couplers, and coupling gaps having physical dimensions from nanoscale to the order of optical wavelengths. Integration of photonic devices can be easily achieved through fabrication methods like optical lithography, chemical vapor deposition, and chemical or plasma etching. Dimensions of 100-200 nm are routinely achieved in the manufacturing of integrated circuits (IC). Nanofabrication techniques allow the realization of semiconductor microcavity ring and disk resonators with evanescent wave coupling to micron- or submicron-width waveguides across nanoscale air gaps. With high-quality etching, the scattering loss can be minimized to achieve simultaneously a high *Q* and high finesse. For example, the present authors[11] recently nanofabricated integrated microcavities and waveguides (see Fig. 1) using 248nm optical lithography and conventional silicon IC processing. Zhang et al.[12] realized an InGaAsP photonic-wire microcavity ring laser consisting of a ring cavity of 4.5μm-in-diameter and a curing waveguide of 0.4-μm in width. Laine et al.[13] considered microsphere and waveguide coupler in their acceleration sensor design. Klunder et al.[14] designed laterally and vertically waveguide-coupled cylindrical micro-resonators in $Si_3N_4$ on $SiO_2$ technology using conventional optical

lithography. Krioukov et al.[15] examined integrated optical microcavity sensors. Additionally, these resonators can be integrated with low-threshold photonic-wire microcavity lasers[16] to achieve compactly integrated and robust lab-on-a-chip system.

With size flexibility, mechanical stability, adaptability to integrated circuits, very high quality factor, and very small mode volume, WGM microresonances have become subject of numerous studies in basic research and emerging applications. In a recent review[17] Vahala summarized four applications of optical microcavities: strong-coupling cavity quantum electrodynamics (QED), enhancement and suppression of spontaneous emission, novel sources, and dynamics filters in optical communications. Thus, the vast literature in these four fields is not cited here. In the past decade extensive texts and treaties have been published on microcavity semiconductor lasers[12, 16, 18]. Other topics include microsphere photonics[2], soliton effects[19], chaos[20], narrow filters[21], optical switch[22], high-resolution spectroscopy[15, 23], optical memories[24], and microsensors[13, 25-27], etc.

In a recent parametric study[28], we found that the gap separating the waveguide and the resonator had little effect on the FSR. However, the gap did strongly influence the cavity *Q* factor and the FWHM of the resonant modes. In this treatise, we will investigate the gap effects on the WGM microresonances for two planar microdisk and waveguide coupling systems. The remainder of this paper is organized as follows. Section 2 deals with the theoretical formulation and numerical methodology. Section 3 describes the simulation models, and examines the simulation accuracy and sensitivity. Section 4 discusses the results of the gap effects. We present our conclusions in the last section.

## 2. METHODOLOGY

We used the Helmholtz equations derived from Maxwell's equations and the finite element method to simulate WGM microresonances in planar microdisk-waveguide coupling systems. Under WGM resonances the EM field inside the microdisk is typically an equatorial brilliant ring (for the first-order resonance). And the ring is located on the same plane as the waveguide. Further, the structure of the microdisk is planar. So it is feasible to use a two-dimensional (2-D) theoretical model. The time-dependent Maxwell's equations are

$$\begin{cases} \nabla \cdot \bar{E} = \dfrac{\rho}{\varepsilon}; \quad \nabla \times \bar{E} = -\mu \dfrac{\partial \bar{H}}{\partial t} \\ \nabla \cdot \bar{H} = 0; \quad \nabla \times \bar{H} = \bar{J} + \varepsilon \dfrac{\partial \bar{E}}{\partial t} \end{cases} \tag{2}$$

where $\bar{E}$ and $\bar{H}$ are the electric and magnetic field vectors, respectively; $\varepsilon$ and $\mu$ are the permittivity and permeability of the medium; $\rho$ is the electric charge density; and $\bar{J}$ is the electric current density.

For the electric field, since $\rho = 0$ and $\bar{J} = \sigma \bar{E}$, we can derive the equation for $\bar{E}$ as follows:

$$\nabla^2 \bar{E} - \mu\sigma \frac{\partial \bar{E}}{\partial t} - \mu\varepsilon \frac{\partial^2 \bar{E}}{\partial t^2} = 0 \tag{3}$$

where σ is the electrical conductivity. For time-harmonic waves,

$$\bar{E}(\bar{r},t) = \bar{E}'(\bar{r}) e^{i\omega t}. \tag{4}$$

Equation (3) is then simplified to a Helmholtz equation:

$$\frac{1}{\mu} \nabla^2 \bar{E} + \omega^2 \varepsilon_c \bar{E} = 0 \tag{5}$$

where we have introduced the complex permittivity $\varepsilon_c = \varepsilon_{cr} \cdot \varepsilon_0 = \varepsilon - i(\sigma / \omega)$ and $\omega = 2\pi c / \lambda$; $c$ is the speed of light in the medium and $\lambda$ is the light wavelength. Here, the complex index of refraction, $m = n - ik$, is conveniently introduced for the treatment of wave propagation; $n$ is the real part of the refractive index and represents a spatial phase change of the electromagnetic wave; $k$ is the absorption index and stands for a spatial damping on the electromagnetic wave. The relationship between $\varepsilon_{cr}$ and $m$ is expressed by

$$\varepsilon_{cr} = m^2 = n^2 - k^2 - i2nk. \tag{6}$$

Similarly we can get a Helmholtz equation for the magnetic field:

$$\frac{1}{\mu}\nabla^2\overline{H} + \omega^2\varepsilon_c\overline{H} = 0 \tag{7}$$

In the present calculations we consider the In-plane TE waves, where the electric field has only a z-component; and it propagates in the x-y plane. Thus, the fields can be written as:

$$\overline{E}(x,y,t) = E_z(x,y)\overline{e}_z e^{i\omega t} \quad \overline{H}(x,y,t) = [H_x(x,y)\overline{e}_x + H_y(x,y)\overline{e}_y]e^{i\omega t} \tag{8}$$

At the interface and physical boundaries, the natural continuity condition is used for the tangential component of the magnetic field, i.e.,

$$\overline{n}\times\overline{H} = 0\,. \tag{9}$$

For the boundaries of the calculation domain, the low-reflecting boundary condition is adopted. The low-reflecting condition means that only a small part of the wave is reflected, and that the wave propagates through the boundary almost as if it were not present. This condition can be formulized as

$$\overline{e}_z \cdot \overline{n}\times\sqrt{\mu}\overline{H} + \sqrt{\varepsilon}E_z = 0\,. \tag{10}$$

The light source term $E_{0z}$, which propagates inwards through the entry of the waveguide, was treated as an electrically low-reflecting boundary expressed by

$$\overline{e}_z \cdot \overline{n}\times\sqrt{\mu}\overline{H} + \sqrt{\varepsilon}E_z = 2\sqrt{\varepsilon}E_{0z}\,. \tag{11}$$

The quality factor $Q$ is expressed by:

$$Q = \omega_0/\Delta\omega = 2\pi\omega_0\tau \tag{12}$$

where $\omega_0$ is the central frequency of a resonant band, $\Delta\omega$ is the resonance linewidth, and $\tau$ is the photon lifetime.

The In-plane TE waves application mode of the commercial FEMLAB package (version 3.0) was employed for the finite element analysis. In order to solve the problem using the FEM, we need to convert the foregoing strong formulation to a weak form. By applying the Galerkin method to Eqs. (5) and (7), the integral form of the equations is obtained as:

$$\int_\Omega W\cdot(\frac{1}{\mu}\nabla^2\Phi + \omega^2\varepsilon_c\Phi)d\Omega = 0 \tag{13}$$

where $\Phi$ is a set of trial function ( approximation of $E_z$ ) that satisfies the boundary conditions, $W$ is a weighting or test function, and $\Omega$ is the computational domain. Integrating the first term of Eq. (13) by parts results in

$$\int_\Omega(\frac{1}{\mu}\nabla W\cdot\nabla\Phi - \omega^2\varepsilon_c W\cdot\Phi)d\Omega - \oint_\Gamma\frac{1}{\mu}W\frac{d\Phi}{dn}d\Gamma = 0 \tag{14}$$

where $\Gamma$ is the boundary of the domain. Now we use the basic shape function $N$(x, y) to expand $\Phi$ and $W$ :

$$\Phi = \sum_{i=1}^{n} N_i E_{Zi}\,,\ E_Z' = \frac{d\Phi}{dn} = \sum N_i E_{Zi}'\,,\quad W = \sum_{i=1}^{n} N_i\,. \tag{15}$$

Here $n$ is the number of nodes and subscript $i$ represents the node order. The numerical discretization is completed with the enforcement of Eq. (14) for all finite elements. Substituting Eq. (15) into Eq. (14) results in the following matrix formation:

$$[S][E_Z] - [T][E_Z'] = 0 \tag{16}$$

with

$$[S] = \sum_{all-element}\int_{\Omega_e}(\frac{1}{\mu}\nabla N^T\cdot\nabla N - \omega^2\varepsilon_c N^T\cdot N)d\Omega \text{ and } [T] = \sum_{all-boundary-elements}\int_{\Gamma_e}\frac{1}{\mu}N^T\cdot N d\Gamma \tag{17}$$

where $N$ is a row vector, $\{N_1, N_2, \ldots\}$, and $N^T$ is a transpose vector of $N$. The line integral in Eq. (17) needs to be evaluated only over elements that have a side in common with the boundaries of the problem. Normally this integral is simply set to zero, which gives the so-called natural boundary condition. The basis of polynomial functions $N$(x, y) gives an approximation of the solution into the element.

## 3. SIMULATION MODELS AND ACCURACY

As above mentioned, two microdisk and waveguide coupling systems are considered in this study. One of the systems is referred as the 10μm-diameter microdisk system, in which a microdisk of 10μm in diameter is coupled with a waveguide of 2μm in width. Another one is named as the 2μm-diameter microdisk system, in which a microdisk of 2μm in diameter is coupled with a waveguide of 0.5μm in width. The waveguides are straight. All the microdisks and waveguides are made of the same material (silicon nitride) and are assumed to have a constant refractive index of 2.01 against the excitation wavelengths (600 – 850nm) and lossless. The surrounding medium in the systems is air. The gap is defined as the narrowest distance between the microdisk and the waveguide in a system. The gap varies from zero (in close contact) to 1000nm.

Each system is modeled as a rectangular simulation domain. The dimensions of the simulation domains are 4μm×5.5μm and 14μm×16μm for the 2μm- and 10μm-diameter microdisk systems, respectively. The domains were meshed by many triangle elements generated automatically by the FEMLAB software in which a mesh gradient approach was adopted to deal with abrupt changes in sensitive areas like the vicinity around the periphery of the microdisk and the gap region. However, such an approach was not very satisfactory because there is no constant gradient change in the resonant EM field existed inward from the periphery of the cavity. To meet with this requirement, we divided the microdisk into two regions and used hierarchical meshing to scale the cavity down to two different spatial levels: a ring where resonant EM field exists and an inner disk. The mesh in the ring is then locally refined. Exemplary meshes for the two simulation domains are shown in Fig. 2. Since the 2μm-diameter microdisk has a large curvature, energy "leakage" from the cavity surface due to scattering could be appreciable. Therefore, we considered an additional ring surrounding the 2μm-diameter microdisk. The mesh in this additional ring is also refined. As shown in Fig. 2, the meshes inside the rings, the gap regions and the small waveguides are finer than other regions.

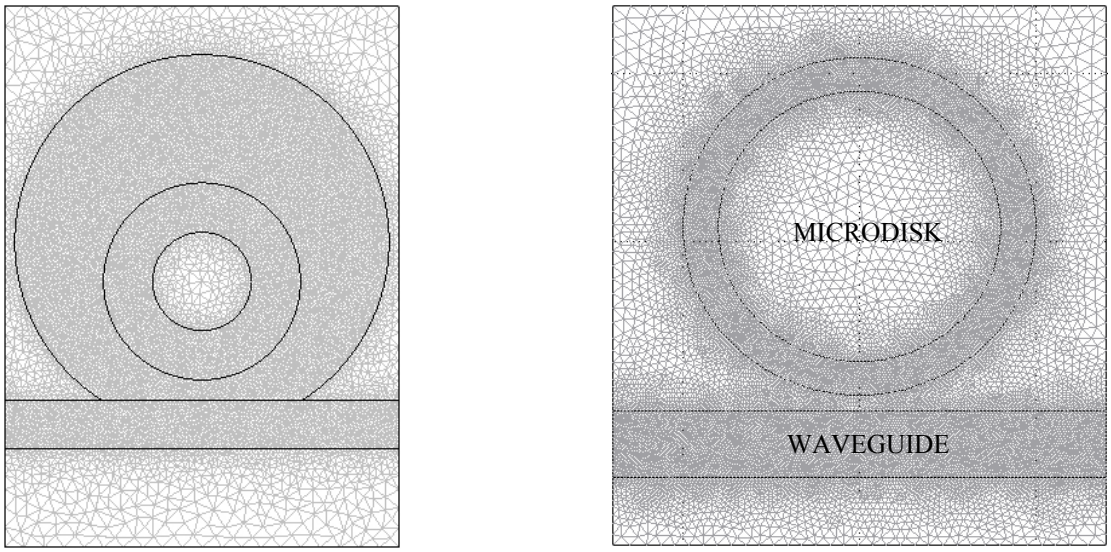


(a) the 2μm-diameter microdisk system (b) the 10μm-diameter microdisk system

Figure 2. The simulation domains and meshes.

Let us examine the simulation accuracy and sensitivity using the 2μm-diameter microdisk system as an example. The considered gap is fixed at 100nm. The concept of the maximum element size $d_{\max}$ is introduced for the sensitive simulation sub-domains including the resonant EM ring, the photon tunneling gap, and the waveguide because of the local refining of meshes. It means that the size of any meshed element in these specific sub-domains should not be

larger than this value. In general, the number of elements generated depends on the $d_{max}$ value used. Smaller $d_{max}$ creates more elements, and requires larger computer memory and longer CPU time. In return, it leads to more accurate simulation results. However, there should be a trade-off between memory consumption, CPU time, and calculation accuracy. In the present calculations, we used a DELL PC equipped with one 2.8 GHz CPU and 2.0 GB memory. The FEMLAB was found to be able to utilize up to 1.5 GB memory under the windows XP operation system. Such a memory usage corresponds to a limit of about $10^5$ elements created in a simulation domain.

We found that when $d_{max}$ equals to 0.04 μm (~1/20 wavelength), FEMLAB generates 104,460 elements for a simulation domain. This smallest $d_{max}$ value is the calculation limit for the PC employed. The simulation result under the limit situation is the most accurate one that we can approach. In Fig. 3 we compare the calculations under larger $d_{max}$ values (then smaller element numbers) with this limit calculation. Fig. 3a shows the relative errors of the stored energy under the first-order resonance around 823 nm in the 2μm-diameter microdisk against the change of the maximum element size. It is evident that the computational error is less than 5% when $d_{max}$ is not larger than 0.1μm (~1/8 wavelength; corresponds to 18,780 elements in the present model). The curve of the stored energy in the cavity vs. the element number used in the whole simulation domain is displayed in Fig. 3b. It is seen that the calculated energy storage inside the disk almost reaches to a constant value after 40,000 elements. Therefore, we can confidently pick up a $d_{max}$ value of 0.05μm (68,560 elements) for the following calculations for the 2μm-diameter microdisk system. The calculation error is as small as 0.18%. Due to the memory limitation of the PC, certainly it is impossible to use such a small $d_{max}$ value for the 10μm-diameter microdisk system which is about 10 times of the area of the 2μm-diameter microdisk system. We selected a value of $d_{max}$ = 0.15 μm (~1/6 wavelength) for the 10μm-diameter microdisk system.

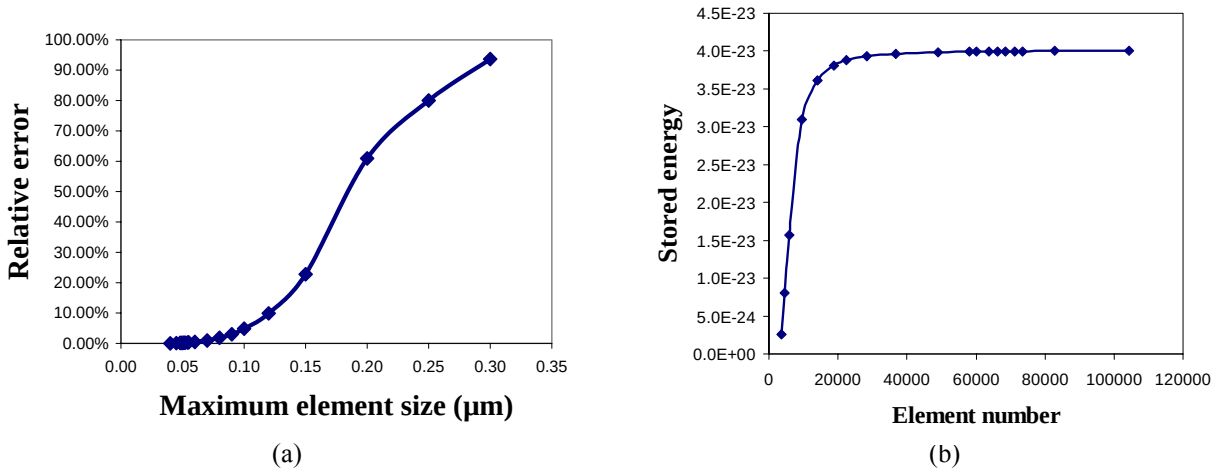


Figure 3. (a) The computational error against the maximum element size; and (b) the convergence curve with respect to the element number used.

The CPU time consumption is basically not a concern for an individual simulation run in the present calculations because each run only took several minutes in the PC. In order to get a resonant spectrum, however, hundreds of simulation runs are needed. In particular, the resonant band is extremely fine for larger gaps due to the high-*Q* characteristic of WGM microresonances. It takes dozens of runs to find a resonant band for each gap value in the WGM systems. The whole simulation can be time-consuming.

## 4. RESULTS AND DISCUSSION

To demonstrate the gap influences on the WGM resonant phenomena, the stored energy inside the resonator is integrated as a main variable used to create the resonant spectrum against the excitation wavelengths; and consequently the resonant spectrum is utilized for finding critical parameters of WGM resonators such as the *Q*-value and FWHM of the resonant mode. Further, the stored energy reflects that how many photons tunnel through the gap from the light-delivery waveguide into the resonant microdisk. It indicates the coupling efficiency of energy transfer. By drawing the curve of the stored energy against the gap change (with a constant intensity of incident radiation) we can find an optimal gap for efficient light coupling.

Figs. 4 a and b show the profiles of the stored energy versus the gap for the 10μm- and 2μm-diameter microdisk systems, respectively. The simulated results are represented by the discrete symbols. The results can be fitted into Lorentz fittings. And then the maximum stored energy for each curve is found. The results of the stored energy are finally normalized by the respective maximum stored energies. In Fig. 4a, we considered two resonant modes: ~ 801nm (near infrared light) and ~ 608nm (yellow light), respectively. In Fig. 4b, only one resonant mode was considered (~ 822nm). The gap varies from zero to 800nm with a step change of 50nm. It is estimated from the fitted curves that the energy storage is the greatest when the gap is about 260nm for the excitation wavelength of 608nm (for the 10μm-diameter microdisk system), about 480nm for the excitation wavelength of 801nm (for the 10μm-diameter microdisk system), and about 180nm for the excitation wavelength of 822nm (for the 2μm-diameter microdisk system), respectively. Such optimal gap values represent the most efficient energy coupling in the respective resonator systems at the respective resonant wavelengths. The results reveal that an optimal gap for highly-efficient coupling does exist and the optimal gap is a function of the resonant mode!

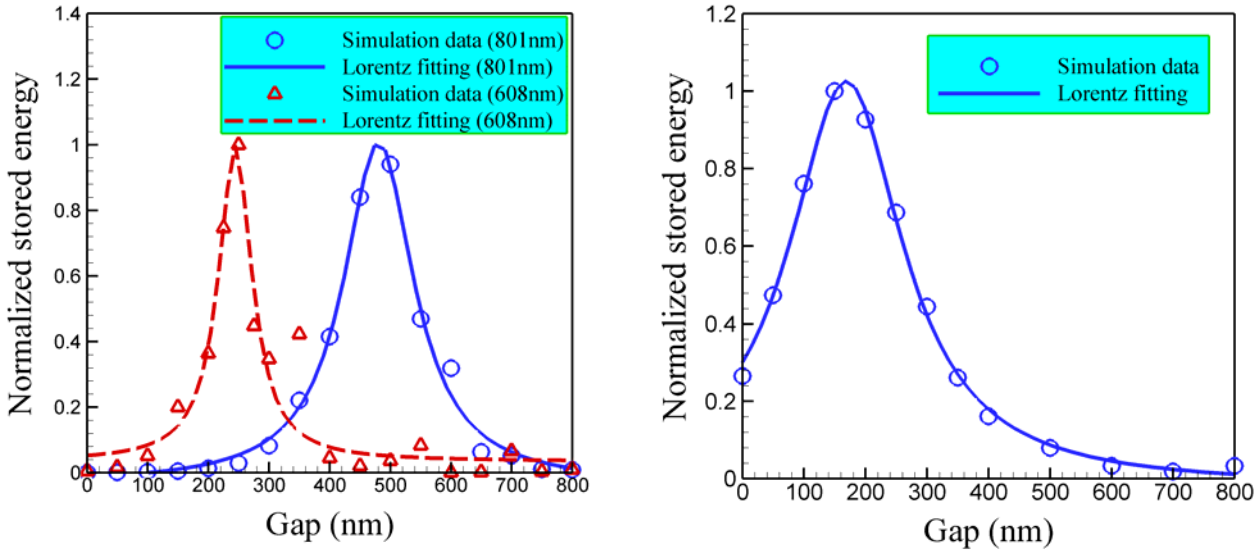


(a) the 10μm-diameter microdisk system

(b) the 2μm-diameter microdisk system

Figure 4. The stored energy (normalized) vs. the gap.

It is easy to understand the reduction of coupling efficiency at gaps larger than the optimal gap, because it is well-known that the evanescent field strength from a surface decays exponentially as a function of the distance to the surface. The longer the distance, the weaker is the strength. The evanescent field is almost negligible at a distance over one optical wavelength involved. How can we understand the reduction of the coupling efficiency for gaps smaller than the optimal gap? From the viewpoint of the evanescent strength, a smaller gap has a stronger strength and closer overlapping of the two evanescent fields from the resonator and the waveguide, respectively. A smaller gap affords more opportunities to photon tunneling. Indeed because of the enhanced photon tunneling, photons confined in the resonator tunnel back to the waveguide. As a result, a narrower gap reduces the coupling efficiency as a system. Therefore, an optimal gap for energy coupling exists as a trade-off between bidirectional coupling efficiencies.

Gorodetsky and Ilchenko[8] experimentally observed a dip in the output intensity of a prism coupler in a fused-silica sphere with increasing gap.

Further inspection of Fig. 4, we found that the full width at half maximum of the stored energy curves is narrow for short resonant wavelengths. Photons in longer wavelengths can tunnel in a broader gap range. Actually, the resonant intensity is a strong function of the mode number (affects the wavelength, see Eq. (1)). At a fixed gap of 300nm in the 10μm-diameter microdisk system, for instance, the absolute value of the stored energy at the 801nm resonant mode is ten times larger than that at the 608nm resonant mode. This indicates that the coupling efficiency for short wavelengths is lower. The result is consistent with the findings by Hagness et al.[29] We conclude that a longer resonant wavelength is preferable in the generation of WGM microresonances because of wider gap latitude in the coupling efficiency and that an optimal gap becomes more critical for shorter resonant wavelengths.

The optimal gap for coupling also depends on the geometric configuration of the resonance system, in particular the curvature of the resonator. Comparing the optimal gaps for the two different resonator systems, clearly a larger curvature (smaller resonator) requires a closer overlapping of the evanescent fields in the gap. Thus, the optimal gap decreases with the decrease of resonator size. In Fig. 4b, the stored energy is relatively appreciable when the waveguide is in close contact (zero gap distance) with the 2μm-diameter resonator; while in Fig. 4a, the stored energy is almost invisible (as compared with the maximum stored energy) when the waveguide is in close contact with the 10μm-diameter resonator.

To better understand the gap effects on the coupling efficiency, we plot in Figs. 5 and 6 the distributions of the electric fields of the simulation systems for different gaps. Three gaps are selected for each simulation system: one is before the respectively optimal gap, one is close to the respectively optimal gap, and one is after the respectively optimal gap. It is seen that the EM fields inside the resonators in Figs. 5b and 6b (with gap close to the optimal values predicted in Fig. 4) are much stronger than those in the other resonators; whereas the EM fields in the waveguides in Figs. 5b and 6b are extremely weak because the majority of the energy is coupled into the resonators. The results in Figs. 5 and 6 also confirmed that the resonant EM field is concentrated inside the inward ring close to the periphery of the resonator and the energy leakage from the 2μm-diameter microdisk is stronger than that from the 10μm-diameter microdisk.

The gap effects on important resonant parameters like the FWHM and *Q* factor of a resonant mode are shown in Figs. 7 a and b for the 10μm- and 2μm-diameter microdisk systems, respectively. The resonant mode is at 801nm for the 10μm-diameter microdisk system and at 822nm for the 2μm-diameter microdisk system. The discrete symbols represent the simulated results and the variations can be fitted into the Boltzmann fittings. We found that with the increase of the gap from zero to 1000nm, the FWHM (unit: GHz) narrows and the *Q* factor increases. The fitted curves show that with the increase of the gap distance, the *Q* factor increases almost exponentially at the beginning before the gap reaches to the optimal gap for coupling; after passing the optimal gap, the increase of the *Q* factor slows down gradually and finally becomes quite flattened. A maximum *Q* factor is reached at a gap about one wavelength of the resonant mode. However, the resonant energy in the resonator is extremely weak at this gap distance as shown in Fig. 4. Simultaneously considering Figs. 4 and 7, we suggest a trade-off between the coupling efficiency and the *Q* factor. For some applications such as WGM-based biosensors and high-resolution spectroscope, it is feasible to sacrifice somewhat of the *Q* factor to guarantee the resonance can be conveniently measured. A gap located at half of the maximum stored energy after the optimal gap for coupling can be chosen as an optimum gap in which both the *Q* factor and coupling efficiency are high.

Comparing Fig. 7a with Fig. 7b, it is seen that the achievable *Q* value for the 10μm-diameter resonator is over three orders of magnitude higher than that for the 2μm-diameter resonator. Hence, the *Q* factor shrinks considerably when the size of the resonator approaches to the resonant wavelength. We also found that the stored energy inside the smaller microdisk decreased several orders of magnitude as compared with the counterpart. Thus, a small resonator has low energy storage capacity and poor *Q* factor. Buck and Kimble[30] indicated that the *Q* factor falls approximately exponentially as the resonator size decreases below 10μm. This agrees with our simple picture of the increase bending loss associated with a smaller microdisk.

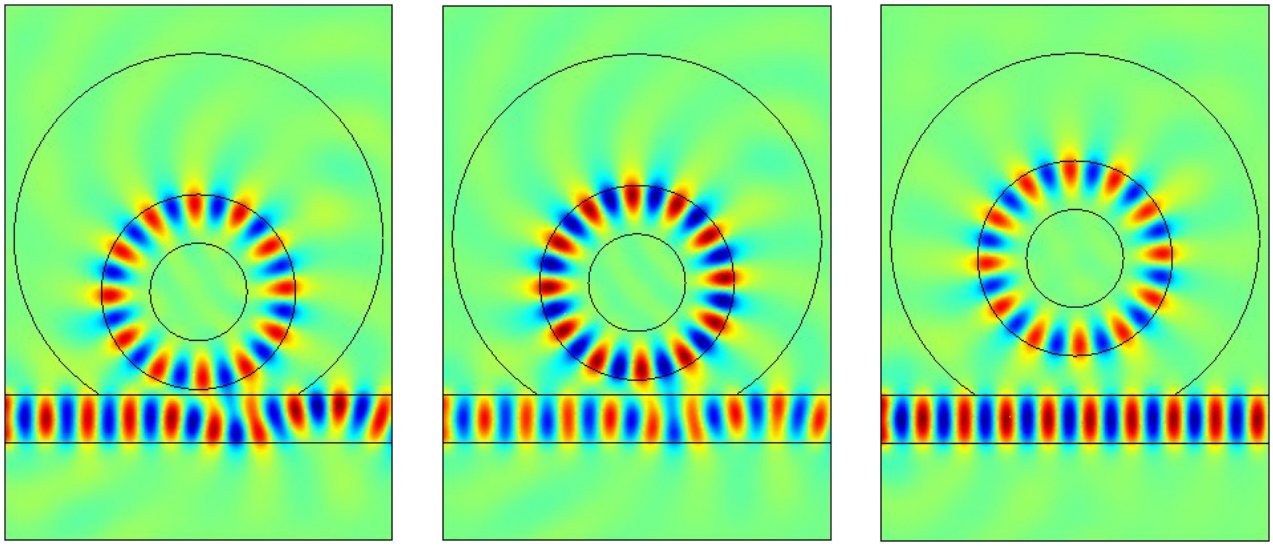

(a) 50nm gap (b) 150nm gap (c) 400nm gap

Figure 5. Electric field distributions for three selected gap values for the 2μm-diameter microdisk system at 822nm.

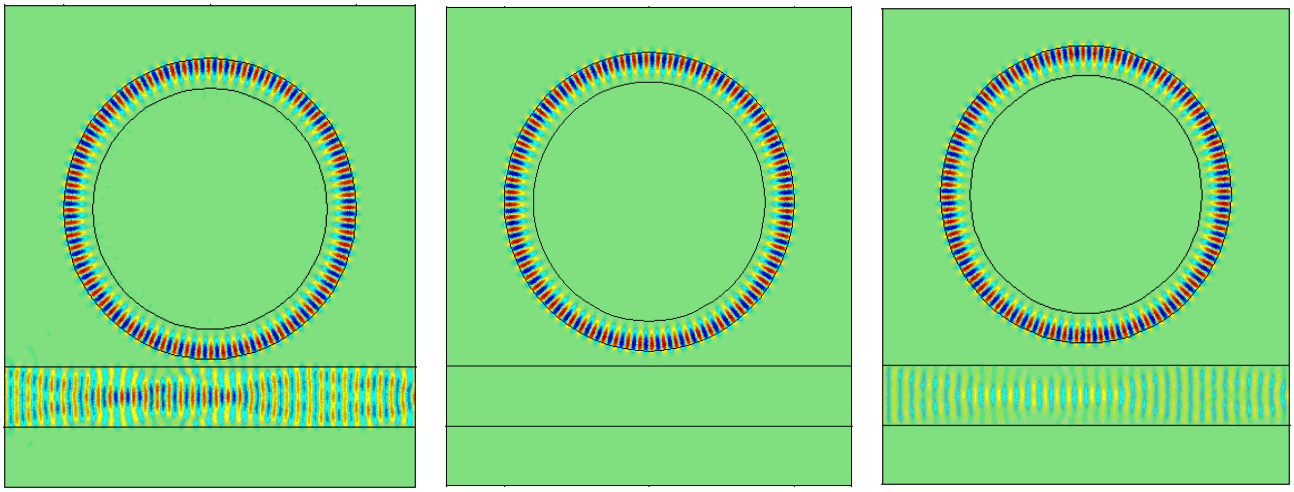

(a) 250nm gap (b) 500nm gap (c) 750nm gap

Figure 6. Electric field distributions for three selected gap values for the 10μm-diameter microdisk system at 801nm.

Figs. 8 a and b show the resonance wavelength shifts against the gap variation for the 10μm- and 2μm-diameter resonator systems, respectively. The shift is defined as $\lambda_g - \lambda_0$, where $\lambda_0$ is the resonance central wavelength under in-contact condition (zero gap) and $\lambda_g$ is the resonance central wavelength corresponding to a gap. It is seen that with increasing gap the resonance wavelength down shifts in Fig. 8a, but up shifts in Fig. 8b. The downshift tendency for the 10μm-diameter resonator system is consistent with the experimental observation[4] in a fused-silica microsphere of 215μm in diameter. However, the reason for opposite up-shift for the 2μm-diameter resonator system remains unclear. The shift could be very appreciable with increasing gap (~ 1nm in Fig. 8). The maximum shift for the small resonator is larger than that for the large resonator. However, the fitted curves indicate that the frequency shifts reach to stable and constant values after the gap distance increases to over 200nm in Fig. 8a and to over 300nm in Fig. 8b. This implies

that the gap after a threshold value will not influence the resonant frequency. This trait is of practical significance for applications using frequency shift characteristic such as in biosensors[7, 26, 27].

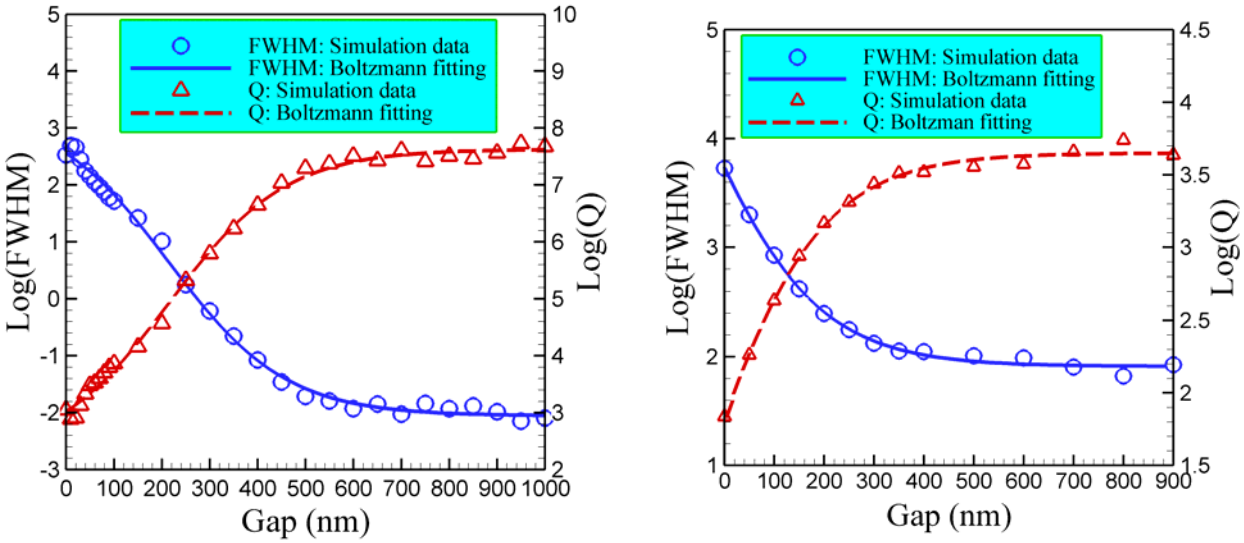


(a) the 10μm-diameter microdisk system (b) the 2μm-diameter microdisk system

Figure 7. Gap effects on the FWHM (GHz) and *Q* factor.

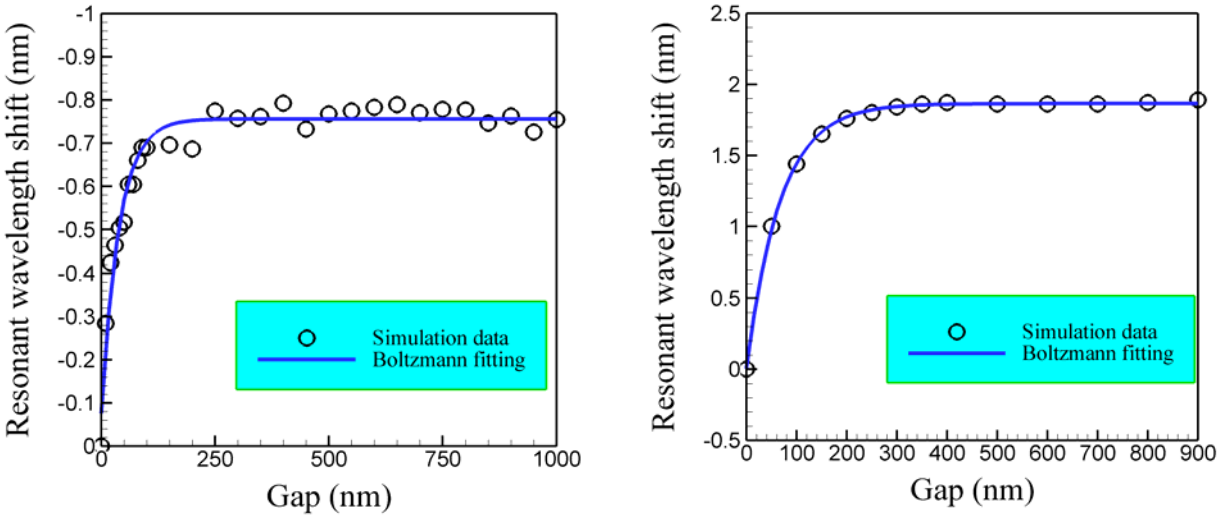


(a) the 10μm-diameter microdisk system (b) the 2μm-diameter microdisk system

Figure 8. Gap effects on the resonant frequency.

## 5. CONCLUSIONS

Nanofabrication techniques allow the realization of semiconductor photonic micro/nanodevices with precise control of the gaps separating microresonators and micron- or submicron-width waveguides. The scattering loss can be minimized to achieve simultaneously a high *Q* and high finesse by etching smooth side wall during fabrication. In this paper, the whispering-gallery mode microresonances were simulated for the two modeling systems with various gaps. The finite element method was employed for the simulations. We first examined the simulation accuracy and sensitivity using the 2μm-diameter microdisk system as an example. It is found that when the maximum element size in the computationally sensitive regions such as the gap, the inward ring close to the cavity periphery, and the waveguide is below 1/8 of the wavelength involved, the computational error is less than 5% as compared to an extreme case.

An optimal gap was found for maximum energy coupling from the waveguide to the resonator. This optimal gap is a strong function of the wavelength of the resonant mode. The shorter the wavelength, the smaller is the optimal gap for coupling. The coupling efficiency is lower for shorter wavelengths. The full width at half maximum of the stored energy curve vs. gap is narrow for short resonant wavelengths. Photons in longer wavelengths can tunnel in a broader gap range. The optimal gap is dependent on the geometric configuration of the resonant system as well. The smaller the cavity size, the narrower is the optimal gap. With increasing gap, the *Q* factor increases; while the FWHM decreases. The *Q* factor increases exponentially at the beginning before the gap reaches to the optimal gap for coupling; after passing the optimal gap, the increase of the *Q* factor slows down; and when the gap approaches to the optical wavelength the *Q* factor is almost maximum and constant. An optimum gap is then suggested at half maximum energy coupling where both the *Q* factor and coupling efficiency are high. For small gaps, the resonance central frequency is strongly affected by the gap. With increasing gap from in-contact to a couple of hundreds of nm, the frequency shift varies exponentially and could reach to the order of 1 nm. For large gaps, the resonance central frequency is not affected by the gap.

## ACKNOWLEDGEMENTS

Z. Guo acknowledges the support of the Academic Excellence Fund Award from Rutgers University and a grant from the National Science Foundation (CTS- 0541585) to the project.

## REFERENCES

1. H.M. Nussenzveig, *Diffraction Effects in Semiclassical Scattering*, Cambridge University Press, New York (1992).
2. S. Arnold, "Microspheres, photonic atoms and the physics of nothing", *American Scientist* **89**, 414-421 (2001).
3. S.C. Hill and R.E. Benner, "Morphology-dependent resonances," *Optical Effects Associated with Small Particles*, P.W. Barber and P.K. Chang, eds, (World Scientific, Singapore; New Jersey; Hong Kong 1988), pp. 3-61.
4. N. Dubreuil, J. C. Knight, D. K. Leventhal, V. Sandoghdar, J. Hare, and V. Lefèvre, "Eroded monomode optical fiber for whispering-gallery mode excitation in fused-silica microspheres," *Opt. Lett.* **20**, 813-815, (1995).
5. L. Collot, V. Lefèvre-Seguin, M. Brune, J. M. Raimond, and S. Haroche, "Very high-Q whispering gallery modes resonances observed on fused silica microspheres," *Europhys. Lett*. **23**, 327-333, (1993).
6. M.L. Gorodetsky, A.A. Savchenkov, and V.S. Ilchenko, "Ultimate Q of optical microsphere resonators," *Opt. Lett.* **21**, 453-455 (1996).
7. H. Quan and Z. Guo, "Simulation of whispering-gallery-mode resonance shifts for optical miniature biosensors," *J. Quantitative Spectroscopy & Radiative Transfer* **93**, 231 – 243 (2005).
8. M. L. Gorodetsky and V.S. Ilchenko, "Optical microsphere resonators: optimal coupling to high-Q whispering-gallery modes," *J. Opt. Soc. Am. B* **16**, pp. 147-154, (1999).
9. A. Serpenguzel, S. Arnold, and G. Griffel, "Excitation of resonances of microspheres on an optical fiber", *Opt. Lett*. **20**, 654-656 (1995).
10. J.C. Knight, G. Cheung, F. Jacques, and T.A. Birks, "Phase-matched excitation of whispering gallery mode resonances using a fiber taper," Opt. Lett., 22, 1129-1131 (1997).

11. H. Quan, Z. Guo, L. Xu, and S. Pau, "Design, fabrication and characterization of whispering-gallery mode miniature sensors", *Nanofabrication: Technologies, Devices, and Applications*, edited by W. Y. Lai, S. Pau, and O. D. López, Proceedings of SPIE Vol. 5592 (SPIE, Bellingham, WA, 2005), pp. 373-381.
12. J.P. Zhang, D.Y. Chu, S.L. Wu, S.T. Ho, W.G. Bi, C.W. Tu, and R.C. Tiberio, "Photonic-wire laser", *Phys. Rev. Lett.* **75**, 2678-2681 (1995).
13. J.P Laine, C. Tapalian, B. Little, and H. Haus, "Acceleration sensor based on high-Q optical microsphere resonator and pedestal antiresonant reflecting waveguide coupler", *Sensors & Actuators A: Physical* **93**, 1-7 (2001).
14. D.J.W. Klunder, E. Krioukov, F.S. Tan, T. Van Der Veen, H.F. Bulthuis, G. Sengo, C. Otto, H.J.W.M. Hoekstra, and A. Driessen, "Vertically and laterally waveguide-coupled cylindrical microresonators in $Si_3N_4$ on $SiO_2$ technology", *Appl. Phys. B* **73**, 603-608 (2001).
15. E. Krioukov, D.J.W. Klunder, A. Driessen, J. Greve, and C. Otto, "Integrated optical microcavities for enhanced evanescent-wave spectroscopy", *Opt. lett*. **27**, 1504-1506 (2002).
16. J.P. Zhang, D.Y. Chu, S.L. Wu, W.G. Bi, R.C. Tiberio, C.W. Tu, and S.T. Ho, "Directional light output from photonic-wire microcavity semiconductor lasers", *IEEE Photo. Technol. Lett.* **8**, 968-970 (1996).
17. K.J. Vahala, "Optical microcavities", *Nature* **424**, 839-846 (2003)
18. M. Cai, Q. Painter, K.J. Vahala, and P.C. Sercel, "Fiber-coupled microsphere laser", Opt. Lett., 25, 1430-1432 (2000).
19. V.B. Taranenko and C.O. Weiss, "Spatial solitons in semiconductor microresonators", *IEEE J. Select. Top. Quantum Elect.* **8**, 488-496 (2002).
20. A.D. Stone, "Wave-chaotic optical resonators and lasers", *Physica Scripta* **T90**, 248-262 (2001).
21. B. E. Little, S. T. Chu, H. A. Haus, J. Foresi, and J. P. Laine, "Microring resonator channel dropping filters", *J. Lightwave Tech.* **15**, 998-1005, (1997).
22. F. C. Blom, D. R. van Dijk, H. J. Hoekstra, A. Driessen, and T. J. A. Popma, "Experimental study of integrated-optics micro-cavity resonators: toward an all-optical switching device," *Appl. Phys. Lett.* **71**, 747-749, (1997).
23. S. Schiller, and R.L. Byer, "High-resolution spectroscope of whispering gallery modes in large dielectric spheres," *Opt. Lett.* **16**, 1138-1140 (1991).
24. M.T. Hill, H.J.S. Dorren, T. de Vries, X.J.M. Leijtens, J.H. den Besten, B. Smalbrugge, Y.-S. Oel, H. Binsma, G.-D. Khoe, and M.K. Smit, "A fast low-power optical memory based on coupled micro-ring lasers," *Nature* **432**, 206-209, (2004).
25. R.W. Boyd, and J.E. Heebner, "Sensitive disk resonator photonic biosensor", *Appl. Opt.* **40**, 5742-5747 (2001).
26. F. Vollmer, D. Braun, A. Libchaber, M. Khoshsima, I. Teraoka, and S. Arnold, "Protein detection by optical shift of a resonant microcavity", Appl. Phys. Lett., Vol. 80, No. 21, pp. 4057-4059 (2002).
27. S. Arnold, M. Khoshsima, I. Teraoka, and F. Vollmer, "Shift of whispering-gallery modes in microspheres by protein adsorption", Opt. Lett., 28, 272-274 (2003).
28. H. Quan, Z. Guo, and S. Pau, "Parametric studies of whispering-gallery mode resonators", *Nanosensing: Materials and Devices*, edited by M. S. Islam and A. K. Dutta, Proceedings of SPIE Vol. 5593 (SPIE, Bellingham, WA, 2004), pp. 593-602.
29. S. C. Hagness, D. Rafizadeh, S. T. Ho, and A. Taflove, " FDTD microcavity simulations: design and experimental realization of waveguide-coupled single-mode ring and whispering-gallery-mode disk resonators," *J. Lightware Tech.* **15**, 2154-2165, (1997).
30. J. R. Buck and H. J. Kimble, "Optimal size of dielectric microspheres for cavity QED with strong coupling," *Phys. Rev. A* **67**, 033806, (2003).